ADVANCED MATERIALS

Supporting Information

for *Adv. Mater.,* DOI: 10.1002/adma.201807313

3D Printed High-Performance Lithium Metal Microbatteries Enabled by Nanocellulose

Daxian Cao, Yingjie Xing, Karnpiwat Tantratian, Xiao Wang, Yi Ma, Alolika Mukhopadhyay, Zheng Cheng, Qing Zhang, Yucong Jiao, Lei Chen, and Hongli Zhu**

Supporting Information

3D Printed High Performance Lithium Metal Microbatteries Enabled by Nanocellulose from Trees

Daxian Cao[1], Yingjie Xing[1], Karnpiwat Tantratian[2], Xiao Wang[2], Yi Ma[1], Alolika Mukhopadhyay[1], Zheng Cheng[1], Qing Zhang[1], Yucong Jiao[1], Lei Chen[2,*], Hongli Zhu[1,*]

[1]Department of Mechanical and Industrial Engineering, Northeastern University, 360 Huntington Avenue, Boston, Massachusetts 02115, United States

[2]Mechanical Engineering Department, Mississippi State University, 224 Carpenter building, Mississippi State, MS, 39762

Experimental Section

1. Material synthesis.

1.1 The preparation of CNF gel: CNF was prepared by 2,2,6,6-tetramethylpiperidine-1-oxyl (TEMPO) mediated oxidation of softwood pulp. The softwood pulp was obtained from the softwood through chemical and mechanical treatments, which includes the delignification to remove the colored matter.[1] First, 50 g of softwood pulp (water content is ~80%) were dispersed in 500 mL distilled (DI) water and stirred for 2 h. After that, 0.16 g of TEMPO (Sigma-Aldrich, USA), 1 g of NaBr (Sigma-Aldrich, USA), and 30 mL of 12.5 wt% NaClO solution (Sigma-Aldrich, USA) were successively added into the dispersion to initiate the oxidation of the cellulose. During the oxidation process, the pH was maintained at 10 by dropping 1 mol L^{-1} of NaOH solution until the color changed from yellow to colorless and pH remained constant. After stirring overnight, the CNF was washed with DI water and then washed

with centrifugation several times until the pH was around 7. The final CNF gel with a concentration of 5.1 wt% was sealed and stored at 5 ℃ for further use.

1.2 CNF ink: To obtain a CNF ink with high viscosity, the as-prepared CNF gel was sonicated in an ice bath in a probe sonicator (400watt, 20kHz, Sonic, USA) at 50% amplitude on and off for 15 minutes. As the dispersion changed from cloudy to transparent, the CNF ink with a concentration of 8.3 wt% was ready.

1.3 CNF/LFP ink: 2 g of the LFP powder (Fisher, USA) was mixed with 20 g of as-prepared CNF dispersion to form a homogenized gel by stirring for 1 h. After that, a similar sonication with CNF ink was performed to increase the viscosity of the CNF/LFP ink.

2. Electrodes preparation

2.1 3D printing process: The printing process was performed using a benchtop robot (Fisnar F4200n) with 3-axis micropositioning stage based on a preprogrammed patterning procedure. The CNF/LFP and CNF inks were stored in separate syringes attached by luer-lok to a micronozzle (150 μm in diameter) and connected with an air-powered fluid dispenser (DSP501N, Fisnar) to control the extrusion and moving speed. During the printing process, the patterns were preprogrammed, and the nozzle pressure and move speed were set as 80 psi and 2 mm s^{-1}, respectively. After printing, the electrodes were frozen in the refrigerator at -20 C first to keep the structure, and then freeze-dried for 2 days to remove water. The obtained products were annealed at 700 ℃ for 2 h under inert gas atmosphere to carbonize the CNF. The c-CNF/LFP electrode and c-CNF scaffold were both obtained according to this procedure. To evaluate the electrochemical performance of the electrode material, planar electrodes were prepared with the same method.

2.2 c-CNF/Li electrode: After carbonization, the printed c-CNF scaffold was used to host the Li. To make the scaffold more lithiumphilic, a thin ZnO layer was coated on the scaffold. The obtained scaffold was immersed in 1 M Zinc Nitride ($Zn(NO_3)_2$) (Fisher, USA) for 10 min, followed by annealing at 240 ℃ for 10 min. After cooling down, it was transferred to the glove box to incorporate the Li ions. Li ribbon (99.9%, Sigma Aldrich) was melted at 250 ℃ first, and the c-CNF was brought in contact with the molten Li to allow Li fusion in. Li slowly spreads into the whole scaffold, and the amount of Li infused can be controlled by controlling the contact time. Finally, the scaffold with Li was obtained and used as the anode.

3. Characterization methods: The morphology of the samples was examined by a Hitachi S4800 SEM operated at 10 kV. TEM images were performed on the JEOL 1010 operated at 200 kV. The X-ray diffraction (XRD) patterns of the samples were recorded for 2θ ranging from 10° to 80° on Rigaku Ultima IV with Cu Kα radiation. Raman spectra were obtained on a LabRam HR800 UV NIR with 532 nm laser excitation. The conductivity of the electrodes was measured using four probe point measurement, where the printed planner sample owns the size of 10 mm*10 mm* 0.4 mm. The rheological properties were measured on a TA-Instruments ARES-G2 rheometer. All the measurements were carried out at room temperature. The weight content of the LFP in c-CNF/LFP was measured with the TGA, which was carried out in air in the range of 20 to 800 ℃ using a Netzsch STA 409 PC (TGA instrument, Germany).

4. Electrochemical characterization

In all the electrochemical measurements, the electrolyte (DodoChem) was 1 M Li bis(trifluoromethanesulphonyl)-imide (LiTFSI) dissolved in DOL/DME (1:1 v/v) with 2 wt.% lithium nitrate. 100 µL of the electrolyte was added in the cell during the assembly. The separator used in coin cells was Celgard 2325 (thickness was 25 µm). The cathode and anode for

the electrochemical performance measurement have the same size. The active material mass loading in cathode was around 2 mg cm^{-2}. A LANDTH 8-channel tester was used to conduct the galvanostatic test. EIS was conducted with a voltage amplitude of 10 mV in the frequency range of 100 kHz to 100 mHz using Biologic SP150 potentiostat.

4.1 The cycling stability test of anode: A symmetric cell was assembled in a CR 2025-type coin cell, with the printed c-CNF/Li electrode acting as the working electrodes and counter electrodes. The cell was measured in repeating discharge/charge at the current density of 5 mA cm^{-2} with the areal charge of 2.5 mAh cm^{-2}. The current density was based on the area of the electrodes. The symmetric cell of Li foil (MTI) was used to compare with c-CNF/Li for the control group. The cycling stability of anodes was evaluated according to the stability of the voltage hysteresis.

4.2 The specific capacity of electrodes: To evaluate the specific capacity of each electrode, CR 2025-type coin cells were assembled, where the printed planner electrodes and Li foil acted as the working and counter electrodes, respectively. For the c-CNF/LFP electrode, galvanostatic tests were performed at a rate of 0.2 C (1 C equals 170 mA g^{-1}). As to the c-CNF/Li anode, the specific current was 100 mA g^{-1}. It should be noted that the mass was based on the whole electrode.

4.3 The full cell performance: The full cell was assembled in CR 2025-type coin cell, where the as-printed planar c-CNF/LFP and c-CNF/Li electrodes were used as cathode and anode, respectively. The specific capacity was measured based on the weight of c-CNF/LFP electrode. The anode to cathode capacity ratio was estimated at 10:1. The rate performance was tested using various C rates ranging from 0.2 C to 10 C. In the long-term test; the dis-/charge rate was 10 C.

Computational Details

1. Printability of CNF

The required extrusion pressure as a function of the viscosity of the CNF ink.

During the 3D printing process, CNF ink forms a consistent bead geometry, which should be able to maintain dimensional tolerances over time. Further, as a conservative estimate for geometry stability, the extruded material must support the weight of the deposited bead during the processing time. For CNF ink, this stability is required enough viscosity to hold the deformation in an accepted range. Thus, based on Maxwell model[3], as a non-Newtonian, shear-thinning, viscoelastic material, the viscosity of CNF-ink should satisfy:

$$\eta > \frac{\sigma_h}{\left(\varepsilon_0 - \sigma_h / G'\right)} t_p \qquad (1)$$

where ε_0 is the acceptable deformation that generally be taken as ε_0=10%, G' is the storage modulus, σ_h is hydrostatic pressure: $\sigma_h = \rho_{melt} \cdot g \cdot h$, $\rho_{melt} \approx \rho_{water}$ (thickness, h ≈ 0.2 mm for a single layer) and t_p is the characteristic processing time. Notice that the characteristic processing time is the time between the material extruded from nozzle and the stable status (e.g., liquid → solid), which depends on material properties. Hence, based on a conservative estimate, we take t_p = 20s, same as time of printing a single layer.

The elastic deformation, σ_h/G', is assumed to occur immediately, but the strain deformation of viscous part will continue to evolve over time. If the total strain deformation beyond 10%, the deposited layer fails to satisfy geometry accuracy. Also, if the elastic strain σ_h/G' > ε_0, the material immediately fails. Hence, from Eq. (1) and our experiment inputs, we can obtain that

the viscosity of CNF-ink, η, should be larger than 400 Pa·s^{-1} to hold structure stable during printing.

Meanwhile, a suitable nozzle extrusion pressure, p, is needed to successfully print CNF with a certain viscosity. Since CNF-ink is the viscoelastic fluid, the viscosity, η, is also related to the shear rate, $\dot{\gamma}$, following a power law relationship, η=C $\dot{\gamma}$ (n-1). Therefore, in order to meet the shear rate through a given nozzle, a corresponding volume flow rate, Q, is required, as calculated by $Q = \dot{\gamma}\pi R^3 n/(3n+1)$[4], in which, R is the radius of nozzle (75 μm), n is the power index (we take n ≈ -0.59 based on Figure 1f).

Finally, the pressure required to successfully extrude a shear-thinning fluid at a given shear rate through a nozzle can be calculated by [4]

$$\mathrm{p} = 8\eta \cdot \mathrm{Q} \cdot \mathrm{L} / \left(\pi \mathrm{R}^4\right) \tag{2}$$

where L ≈ 1.5 cm as the nozzle length. Need to mention that we use 80 psi during 3D printing, which means if we want to extrude CNF-ink successfully, the calculated pressure, p, cannot be larger than the system pressure. If the extrusion pressure is lower than calculated one, CNF-ink cannot be extruded at desired volumetric throughput, or the nozzle may clog.

In order to meet printable criteria, as given in **Figure 1i**, we plot the required extrusion pressure as a function of viscosity of CNF ink. The curve (blue) and dash lines divide plot into five regions. The minimum printable requirement for CNF-ink is η = 400 Pa·s with the corresponding extrudable pressure,14.5 psi, or 100kPa, (red). However, since the maximum system pressure is 80 psi, or 551 kPa, it only allows a maximum viscosity 40000 Pa·s, (green). Thus, the region (i) (80 psi>p>14.5 psi, 40000 Pa·s>η> 400 Pa·s) is the printable zone for 3D

printing CNF-ink by our extrusion system. The region (ii) means the system cannot provide the extrusion pressure larger than 80 psi; the regions (iii), (iv) and (v) those below the curve, the system pressure cannot guarantee the desired volume flow rate for successful extrusion.

The strain deformation of previously deposited layer as a function of nozzle diameter.

The experimental observation shows that when using a large nozzle, e.g., with a diameter of D_E=250 μm, the previously deposited layer undergoes a large deformation leading to geometric inaccuracy. Thus, in this section, we mainly discuss the relationship of the nozzle diameter and the resulting deformation of the deposited layer.

A previously deposited layer generally holds and provides a suitable rigid substrate for the next deposited layer. Therefore, there is a combined stress acting on the previously deposited layer, as[2]

$$\sigma_s = \sigma_v + \sigma_c \quad (3)$$

The first term σ_v is the stress to re-direct CNF flow from the vertical extrusion nozzle to the horizontal bead bed, defined as

$$\sigma_v = 0.5 \cdot \rho_{melt} \cdot V_E \quad (4)$$

where V_E is the extrusion velocity, expressed as $V_E = Q/(\pi/4)/D_E^2$ [2].

The second term σ_c is the stress due to the compression of the current deposited layer, as $\sigma_c = \pi \cdot Q \cdot \eta \cdot (Q - h \cdot V_E \cdot D_E)/(w \cdot D_E^2 \cdot h^2 \cdot V_h)$, in which V_h is the nozzle moving velocity[2] and w is the width of bead (we take $w = D_E$ for a simple condition). Notice that the time for the compression is given as $t_{comp} = D_E / V_h$ [2], which is a function of the nozzle diameter because we set V_h as a constant during the process.

Here, the strain ε is calculated based on the Maxwell model[2]. We take a strain limit as $\varepsilon <$ 10% for a geometry accuracy criterion. Notice we have not obtained the exact value of yielding

stress, σ_{yield}, we assume the deposited layer would not yield ($\sigma_{yield} >> \sigma_s$). Besides, the rest of parameters are constants, i.e., the viscosity η = 400 Pa·s and a nozzle moving velocity, V_h = 2 mm·s^{-1}.

Figure 1h shows the strain, ε, of the previously deposited layer varies as a function of the nozzle diameter, D_E, at different applied extrusion pressures. Generally, increasing D_E results in a higher strain to the previously deposited layer. Also, the strain deformation is proportional to the applied extrusion pressure. When the applied extrusion pressure is p=20 psi (red line), the deformation of the previously deposited layer is below the defined limit, despite of D_E reaches 250 μm. However, if the applied pressure increases is 40 psi (green), the strain exceeds the defined limit, when the nozzle diameter D_E > 240 μm. Further increasing the applied extrusion pressure, the critical nozzle diameter decreases e.g., in the case of p=60 psi (blue), and p=80 psi (black), the deformation exceeds the deformation exceeds the limit when D_E > 208 μm and D_E > 180 μm, respectively. This is because the pressure contributes to the volume flow rate, which increases the velocity of material extrusion, V_E that in turn brings a higher σ_v, based on Eq. (4).

2. Dendrite suppression

The Li deposition morphology evolutions during plating are simulated by using the non-linear phase-field model developed by L. Chen.[5] The model accounts for the electrodeposition system ($Li^+ + e \rightarrow Li$) where the electrode is Li metal, and the electrolyte consists of cation Li+ and anion $TFSI^-$. In this work, the phase field parameter (ξ) is used to describe two distinct phases: $\xi = 0$ is for the electrolyte, $\xi = 1$ is for the Li metal anode, and any value between 0 and 1 is associated with the interfacial region. Generally, for the electrodeposition, the driving force is usually smaller than the driving force from electrode reactions due to the interfacial energy, when the system is far from equilibrium. Thus, the model considers that the spatiotemporal evolution of the phase field parameter is linearly proportional to the interfacial energy and

exponentially to the thermodynamic driving force related to the electrode reactions, which can be expressed as,

$$\frac{\partial \xi}{\partial t} = -L_\sigma \left(g^{'}(\xi) - \kappa \nabla^2 \xi \right) - L_\eta g^{'}(\xi) \left\{ \exp\left[\frac{(1-\alpha) n F \eta_a}{RT} \right] - c_+ \exp\left[\frac{-\alpha n F \eta_a}{RT} \right] \right\}, \quad (1)$$

where $h(\xi) = \xi^3(6\xi^2 - 15\xi^3 + 10)$ is an interpolating function, L_σ is the interface mobility, and L_η is the reaction-related constant, and $\eta_a = \Delta\phi - E^\theta$ is the activation overpotential (E^Θ is the standard half-cell potential). For simplicity, the movement of Li-ion is only considered. The Li-ion concentration (c_+) is governed by Nernst-Plank Equation, which describes ions moving under the influence of electrostatic force and diffusion, written as

$$\frac{\partial c_+}{\partial t} = \nabla \cdot \left[D^{eff} \nabla c_+ + \frac{D^{eff} c_+}{RT} n F \nabla \phi \right] - \frac{c_s}{c_0} \frac{\partial \xi}{\partial t}, \quad (2)$$

where $D^{eff} = D^e h(\xi) + D^s(1 - h(\xi))$ is the effective diffusion coefficient, D^e and D^s are the Li-ion diffusion coefficients in the electrode (very small), and in the electrolyte, respectively. The source term on the right-hand side corresponds to the local accumulation/consuming rate of Li-ion due to electrochemical reactions at the electrode interface. Lastly, the electric potential (ϕ) is governed by Poisson equation, that is

$$\nabla \cdot [\sigma^{eff} \nabla \phi] = I_R, \quad (3)$$

where $\sigma^{eff} = \sigma^e h(\xi) + \sigma^s(1 - h(\xi))$ is the effective conductivity depending on the phase parameter, σ^e is the conductivity of the electrode, and σ^s is the conductivity of the electrolyte solutions. The source term I_R is associated with charges entering/leaving due to the reaction rate at the electrode interface, having a form of $I_R = nFc_s \partial\xi/\partial t$.

The Li deposition simulations are performed on COMSOL Multiphysics 5.3, the finite element software. The adaptive mesh is selected to capture the moving interfaces accurately, and the minimum grid spacing is 0.2 μm. The 2D porous structure is randomly created with approximate pore sizes of 20-40 μm in the 100 x 100 μm domain. For Li foil, the domain size is 250 x 250 μm. Simulation parameters, which are listed in Table 1, are selected based on the previous publications. For initial conditions, the Li nucleation sites are homogeneous over the porous surface, while the non-homogenous nucleation sites, resulting from the large volume change during cycling are designed on the Li foil surface. The initial Li-ion concentration in the electrolyte domain is 1 mol/m^3 (normalized value c = 1). The initial electric potential over the electrolyte domain and the Li metal anode are 1 and 0 V, respectively, to reflect the electrode-electrolyte potential difference of -1.0 V. The Dirichlet boundary conditions for Eq. (2) and Eq. (3) are set on the opposite side of Li metal anode with the Li-ion concentration of 1 mol/m^3 and the electric potential of 1.0 V, respectively, to account for the bulk electrolytes.

Table 1. Simulation parameters and their normalized value.[5-6]

Parameters	**Real Value**	**Normalized value**
Interfacial mobility, L_σ	0.33 x 10^{-6} m^3/(J s)	2000
Reaction constant, L_η	1.0/s	4000
Gradient energy coefficient, κ	1.5 x 10^{-4} J/m	0.01
Li^+ diffusivity in Liquid, D^s_{Li+}	7.5 x 10^{-10} m^2/s	30
Li^+ diffusivity in electrode, D^e_{Li+}	7.5 x 10^{-13} m^2/s	0.03
Electrolyte conductivity, σ^s	1 S/m	100
Electrode conductivity, σ^e	1 x 10^7 S/m	10^9
Interfacial energy, γ_N	0.9 J/m	0.01
Site density of Li metal, c_s	7.64 x 10^4 mol/m^3	-

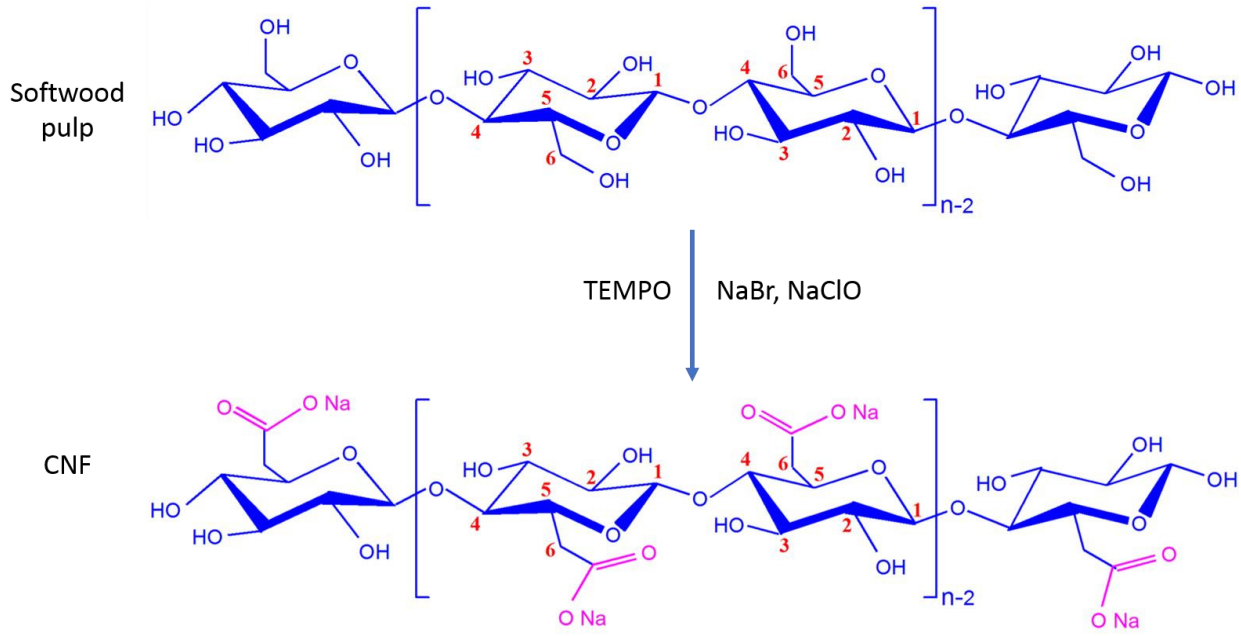

Figure S1. Schematic of the TEMPO treatment process to prepare the CNF and show the abundant hydroxyl and carboxyl groups.

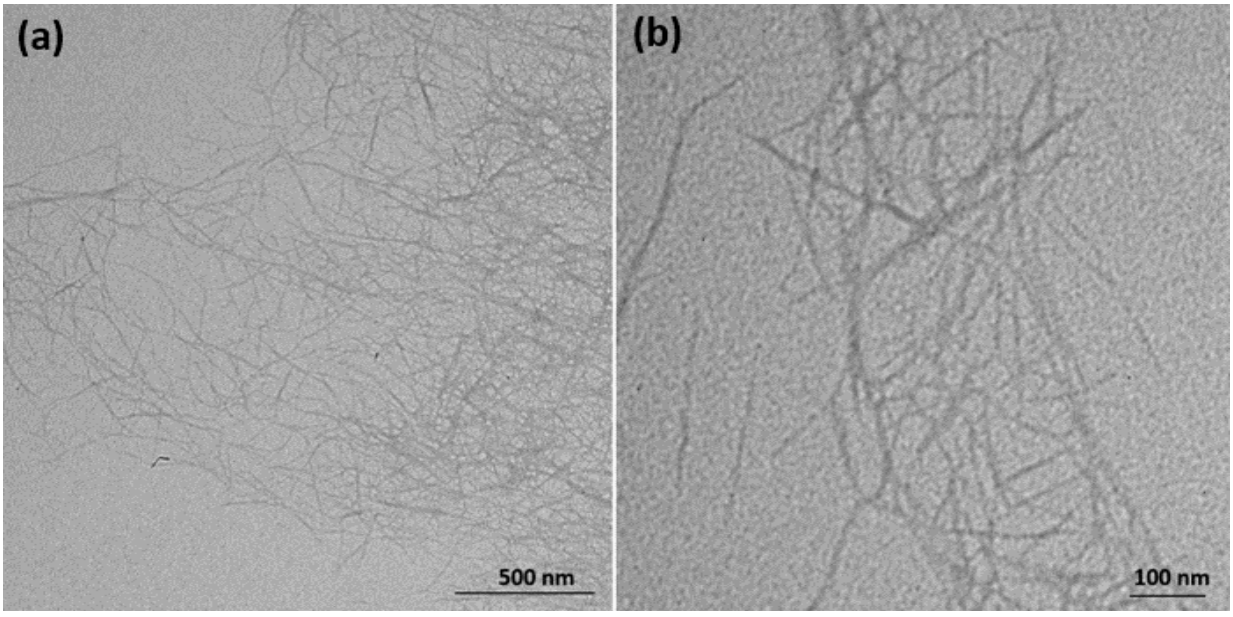

Figure S2. Transmission electron microscope (TEM) images of the CNF to show the length in micrometer and width in nanometer.

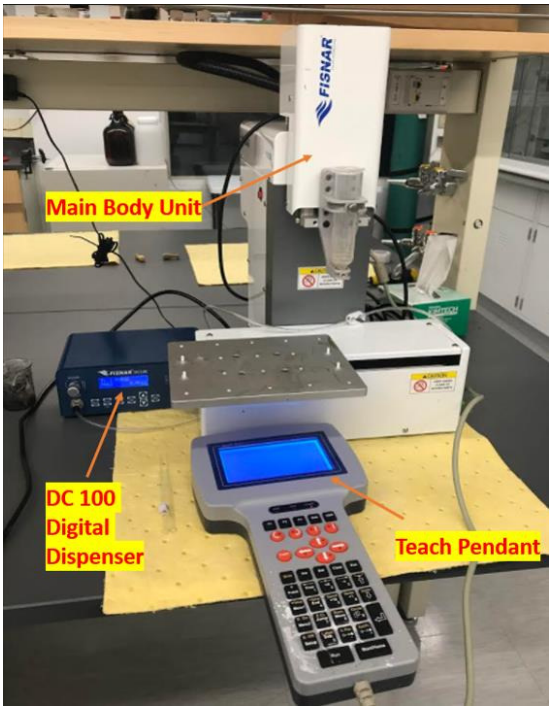

Figure S3. The digital image of the 3D printer.

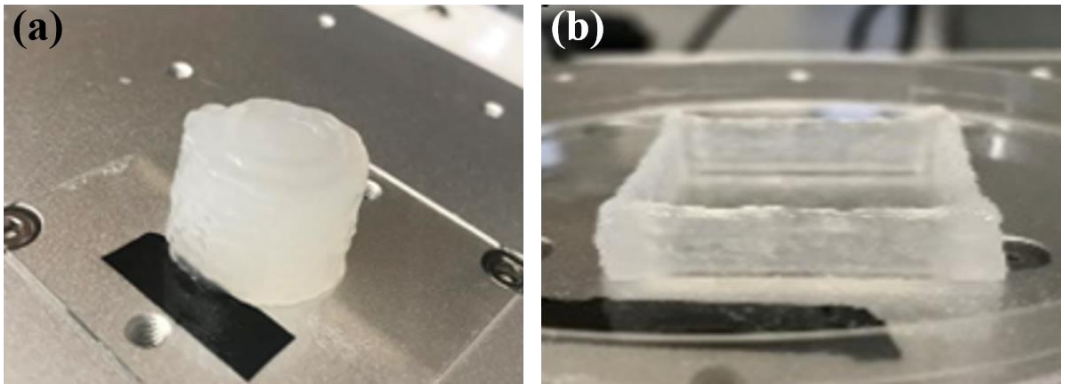

Figure S4. 3D printed (a) spiral cylinder and (b) square structure with the CNF ink.

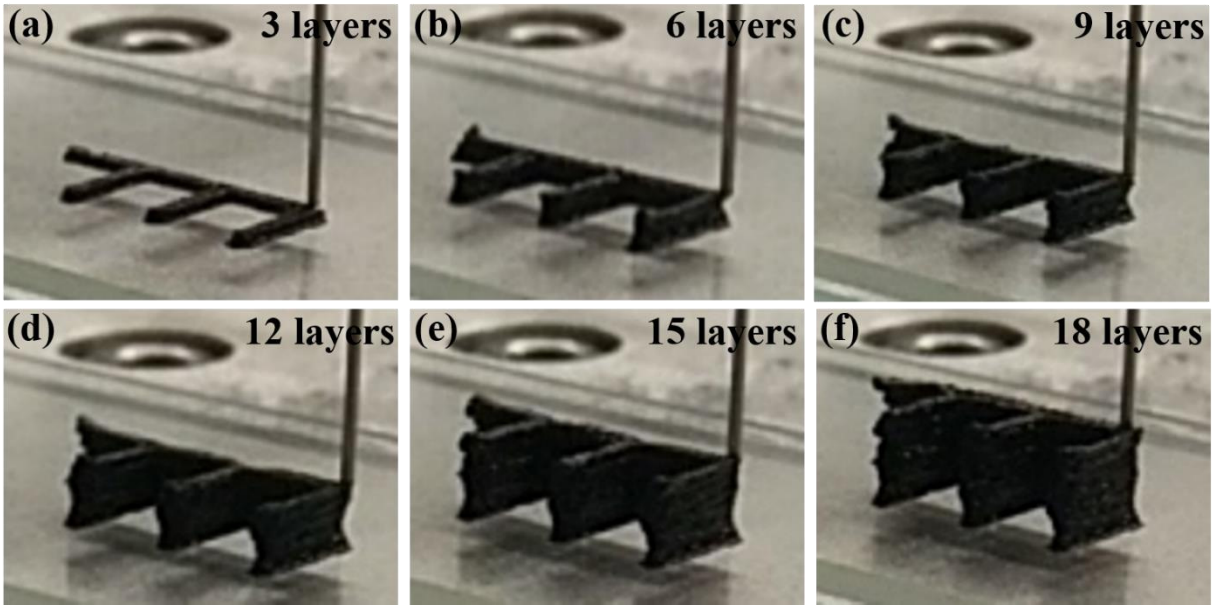

Figure S5. The 3D printing process of cathode part with CNF/LFP ink.

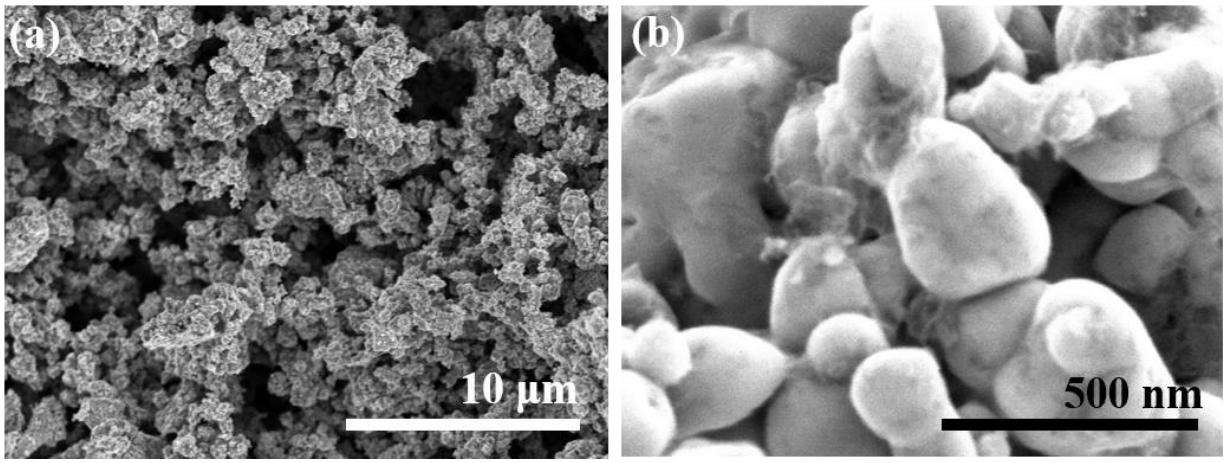

Figure S6. SEM images of LFP particles.

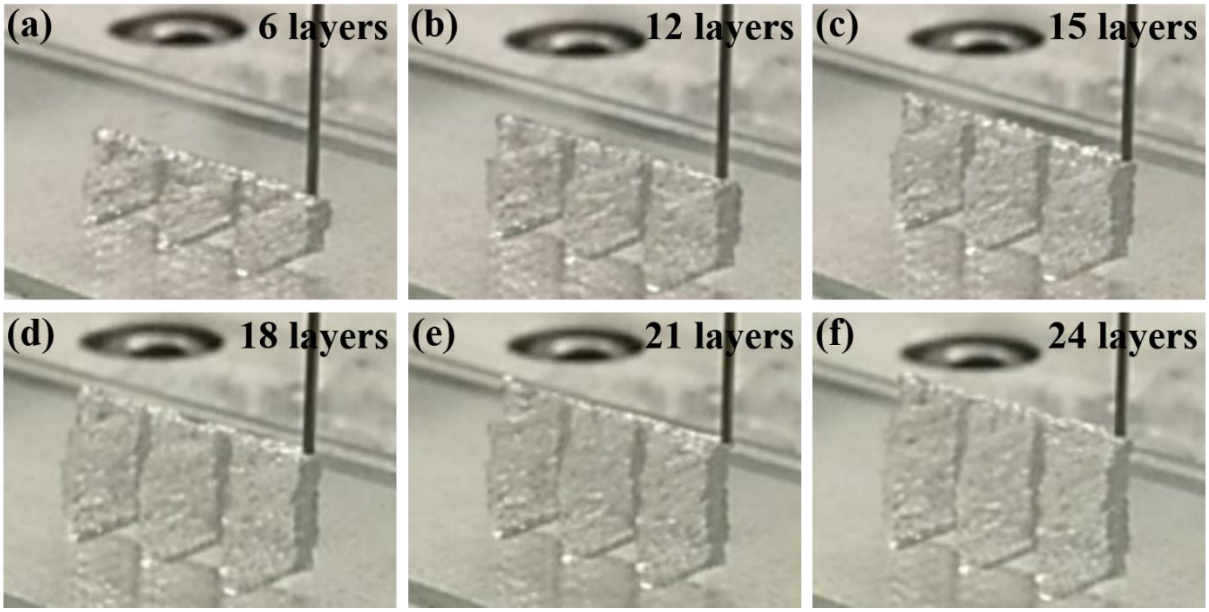

Figure S7. The 3D printing process of anode scaffold with CNF ink.

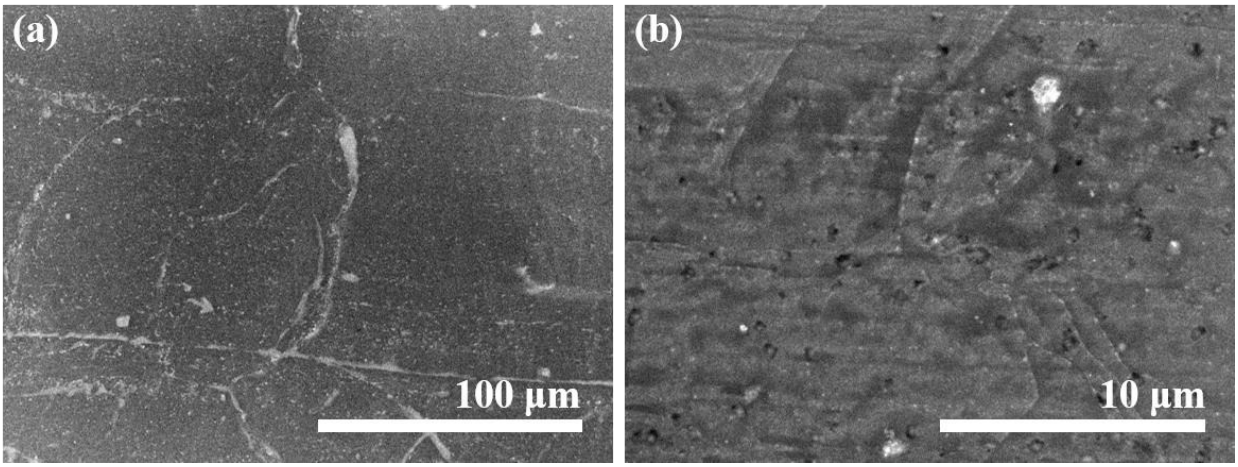

Figure S8. SEM images of Li foil before cycling.

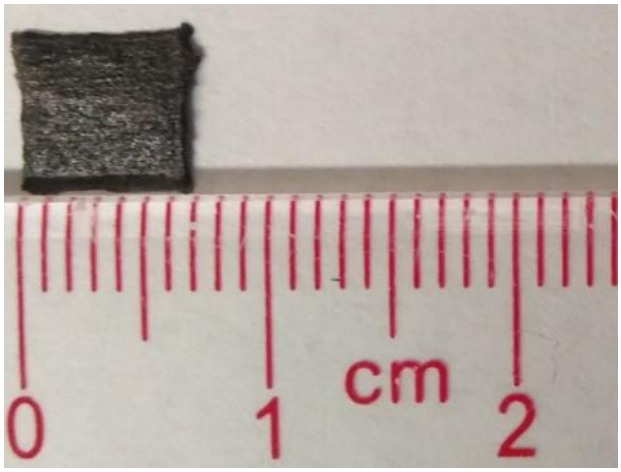

Figure S9 Digital image of Planner electrode with two layers.

[1] H. Zhu, Z. Xiao, D. Liu, Y. Li, N. J. Weadock, Z. Fang, J. Huang, L. Hu, *Energy & Environmental Science* **2013**, 6, 2105.
[2] F. M. White, McGraw-hill, 1986.
[3] J. H. Aklonis, W. J. MacKnight, M. Shen, W. P. Mason, *Physics Today* **1973**, 26, 59.
[4] J. Dealy, K. Wissbrun, Kluwer Academic Publishers.
[5] L. Chen, H. W. Zhang, L. Y. Liang, Z. Liu, Y. Qi, P. Lu, J. Chen, L.-Q. Chen, *J Power Sources* **2015**, 300, 376.
[6] H. H. Yan, Y. H. Bie, X. Y. Cui, G. P. Xiong, L. Chen, *Energy Conversion and Management* **2018**, 161, 193.